Mapp Anna (Orcid ID: 0000-0003-0791-8327)

Electron-deficient p-benzoyl-L-phenylalanine derivatives increase covalent chemical capture yields for protein-protein interactions

Cassandra M. Joiner[1,2, ‡,] Meghan E. Breen[2, ‡], Anna K. Mapp[1,2,3*]

1 Department of Chemistry, University of Michigan, 930 N. University, Ann Arbor, MI 48109
2 Life Sciences Institute, University of Michigan, 210 Washtenaw Ave., Ann Arbor, MI 48109
3 Program in Chemical Biology, University of Michigan, 210 Washtenaw Ave., Ann Arbor, MI 48109

Dedication We dedicate this work to Professor Ronald Raines on the occasion of his 60th birthday. The use of physical organic principles to dissect complex biological problems by Professor Raines serves an inspiration.

ABSTRACT

The photoactivatable amino acid p-benzoyl-L-phenylalanine (pBpa) has been used for the covalent capture of protein-protein interactions (PPIs) *in vitro* and in living cells. However, this technique often suffers from poor photocrosslinking yields due to the low reactivity of the active species. Here we demonstrate that the incorporation of halogenated pBpa analogs into proteins leads to increased crosslinking yields for protein-protein interactions. The analogs can be incorporated into live yeast and upon irradiation capture endogenous PPIs. Halogenated pBpas will extend the scope of PPIs that can be captured and expand the toolbox for mapping PPIs in their native environment.

Keywords: protein-protein interactions, covalent chemical capture, photocrosslinking, p-benzoyl-L-phenylalanine

INTRODUCTION

Transient protein-protein interactions (PPIs) are critical for the precise flow of information in cellular processes, and misregulation of these interactions have been implicated in an array of human diseases.[1-4] There is great interest in methods to successfully detect and characterize these interactions. This is particularly true because the often short (ns-ps) lifetimes and moderate strengths (micromolar to millimolar dissociation constants) of these PPIs makes them difficult to study in their native environment using traditional biochemical techniques.[5-9] With the advance of amber nonsense suppression, photo-activatable unnatural amino acids (UAAs) such as p-benzoyl-L-phenylalanine (pBpa) have been incorporated into proteins and used to capture transient, moderate affinity interactions for mechanistic purposes.[10-28] For example, our lab and others have utilized pBpa to interrogate the interactions involved in a variety of different cellular processes, such as those between transcriptional activators and their coactivator binding partners required for transcriptional initiation and those between chaperones and their substrates required for proper protein folding.[29-34]

pBpa is activated for crosslinking through exposure to UV light (350-365 nm). Upon irradiation, the benzophenone carbonyl undergoes an n to π^* transition to form a diradical species, and the triplet state can abstract hydrogen atoms from activated C-H bonds and recombine to form a covalent adduct [Fig. 1(A)]. If an activated C-H bond is not available, the triplet state will relax back to the ground state and can be reactivated.[35-36] As a result, pBpa undergoes minimal side reactions with solvent, making it particularly useful for in *in vivo*

applications and for interaction surfaces where considerable water is present. However, the low molar absorptivity and quantum yield (ε_{max} < 300 $M^{-1}cm^{-1}$; Φ = 0.05-0.4) of pBpa often limits crosslinking yield. For example, significant starting pBpa-containing protein is often observed in experiments (Fig. S1).

Early mechanistic studies of benzophenone suggest that the incorporation of electron-withdrawing groups (EWGs) onto one or more of the aromatic rings decreases the energy barrier for the n to π^* transition and concomitantly increases the rate of hydrogen atom abstraction.[35-39] Accordingly, we hypothesized that pBpa analogs substituted with electron-withdrawing groups would increase crosslinking yields [Fig. 1(B)]. Here, we demonstrate that halogenated pBpa analogs can be incorporated into live yeast cells using the bioorthogonal *Escherichia coli* tyrosyl tRNA/tRNA synthetase ($tRNA^{TYR}_{CUA}$/TyrRS) system and can capture *in vivo* transcriptional activator-coactivator PPIs. Additionally, the crosslinking yields for EWG-modified pBpa is substantively enhanced.

RESULTS AND DISCUSSION

The design of pBpa analogs containing EWGs was influenced by the crystal structure of the *E. coli* tyrosyl tRNA synthetase that would be used for incorporation.[40] Examination of the structure suggested that the active site would likely accommodate substituents at the para position of the distal ring, but that meta substituents would be more likely to experience steric

clashes (Fig. S2).[41] Seven mono-substituted pBpa analogs containing halogen moieties (Cl, F, Br, and CF_3) at either the meta or para positions of the benzophenone ring were prepared via an air-tolerant carbonylative Suzuki-Miyaura coupling with mono-substituted boronic acids and 4-iodo-L-phenylalanine [Fig. 1(C)].[42,43] The substituted pBpa analogs could be accessed with high purity and excellent yields over 5 steps (see Supporting Information). The incorporation of each analog was assessed in live yeast using the *E. coli* $tRNA^{TYR}_{CUA}$-TyrRS system.[40] We evaluated the incorporation of each analog into the prototypical Gal4 transcriptional activation domain (TAD) at position 849 which has been well characterized for UAA incorporation.[30] Western blotting indicated that all five of the para-substituted analogs were incorporated into LexA-Gal4 at position 849 at levels comparable to pBpa (Fig. 2). As suggested by the crystal structure, substitution at the meta position was not well tolerated and sharp declines in incorporation were observed with substituents larger than fluorine [Fig. 2(C), 2(D)]. Due to the failure of the synthetase to efficiently incorporate the 3-CF_3 Bpa analog, a 3-Br Bpa analog was not prepared for evaluation. These findings are in agreement with previous work by Mehl and others that has demonstrated bioorthogonal tRNA synthetases developed for specific UAAs can incorporate analogs of the cognate UAA without any further mutagenesis to the active site.[42,44-48] Furthermore, this suggests the flexibility of the pBpa specific synthetase could enable the use of a variety of pBpa analogs, particularly those with substitution at the para position.

With the successful incorporation of the analogs, the modified pBpa analogs were assessed for their function as crosslinkers *in vivo* by examining the well-defined PPI between

Gal4 and its masking protein, Gal80. In yeast, Gal4 interacts with the Gal80 repressor through its TAD under normal glucose conditions.[49-51] Our lab has previously demonstrated that pBpa incorporated in either the Gal4 TAD or Gal80 can capture this endogenous interaction in live yeast. Because of the high incorporation yields, the 3-F and 4-F Bpa analogs were selected for comparison with pBpa in this model system. Live yeast expressing a LexA+Gal4 fusion construct with the amber mutation at position 849 and a Myc epitope-tagged Gal80 were grown in glucose in the presence of either pBpa or one of the fluorine analogs [Fig. 3(A)]. Live cells were irradiated with UV light to capture all Gal4 binding partners and were then lysed and immunoprecipitated for the LexA DNA binding domain (DBD) to isolate all LexA+Gal4 protein interactions. To fully characterize the crosslinking abilities of the UAAs, a duplex western blotting strategy was used such that both the binding profile of Gal4 (red) and its direct interaction with Gal80 (green) could be observed on the same western blot (Fig. 3). As seen in Figure 3(B), both fluorine-containing pBpa analogs captured Gal4's endogenous binding partners, including the Gal4-Gal80 interaction (yellow). It was not, however, possible to quantitatively determine a change in crosslinking yield in this system. This is likely due to the high affinity of the Gal4•Gal80 complex, which in turn results in high crosslinking yields with even unmodified pBpa.[49]

To quantitate changes in crosslinking yield, we identified an interaction that was more modest in affinity and that also could be easily examined *in vitro*, thus removing additional variables *in vivo* such as changes in degradation rate that could influence any observations. The

moderate affinity interaction between the VP16 TAD and the Med25 subunit of the Mediator complex was used for this quantitation.[52-53] It has previously been shown that a minimal peptide sequence (441-DFDLDMLG-448) within the N-terminal TAD of VP16 is sufficient for interaction with the Med25 activator interaction domain (AcID) and transcriptional activation.[54-56] We hypothesized that incorporating pBpa at position F442 would not abrogate binding with Med25 AcID and would enable us to observe changes in crosslinking efficiency for the pBpa analogs.

To determine the binding affinities, biotinylated UAA-containing VP16 peptides were incubated with Med25 coated plates. Following incubation with streptavidin-HRP and tetramethylbenzidine (TMB) substrate, the plates were read at 450 nm and it was found that the binding affinities of each pBpa analog containing VP16 peptides were minimally weakened (2-3 fold decrease in affinity) compared to the parent pBpa peptide (Fig. S3).[52,57] These values are in line with the binding affinity of pBpa incorporated VP16 measured by fluorescence polarization (Fig. S4). To evaluate the crosslinking yield, Med25 was incubated with each UAA-containing VP16 peptide at 12.5% of its Kd value to normalize for occupancy. Following 10 minutes of UV irradiation with 365 nm light to covalently capture the interaction, the amount of crosslinked VP16 peptide was quantified by Western blot analysis. As seen in Figure 4, all pBpa analogs gave increased crosslinking yields, and the largest increases were observed with the 3-CF_3 (49-fold increase), 3-Cl (30-fold increase), and 4-CF_3 (23-fold increase) analogs. Similar trends in reactivity for the pBpa analogs were also observed with 1 minute irradiation time (Fig. S5). To

further validate these results, crosslinking yields were also analyzed via ELISA. The biotinylated VP16 peptides were incubated with Med25 coated plates and irradiated with 365 nm light. Following washing and incubation with streptavidin-HRP, the covalently captured VP16 peptide was visualized by addition of TMB substrate [Fig. S6(A)]. Similar trends in reactivity were observed [Fig. S6(B), S6(C)], although the total increase in crosslinking yield is lower. This can be attributed to higher background to the format of the assay. Taken together, our results support the predicted effect of appending electron withdrawing groups onto the benzophenone framework to decrease the excitation energy gap for the n to π^* transition of the carbonyl oxygen's electrons, thereby increasing the reactivity of the benzophenone core and ultimately increasing the crosslinking yield of the molecule.

CONCLUSION

Although pBpa has been shown to have lower reactivity compared to the other common photocrosslinking groups such as the aryl azides and diazarines, its ability to be reactivated and minimal reactivity with solvent makes it a strong tool for the covalent capture of transient PPIs *in vivo*.[14] Therefore, there was a need to increase the crosslinking yield of pBpa to improve the capture of PPIs and accelerate their characterization. Based on previous studies with benzophenones, we hypothesized that pBpa analogs substituted with electron withdrawing groups would increase crosslinking yields. We synthesized seven mono-substituted pBpa analogs (Fig. 1) and showed that upon irradiation of live yeast expressing UAA-containing LexA+Gal4

we capture Gal4's endogenous binding partners, including its masking protein Gal80. Furthermore, we demonstrated *in vitro* the halogenated pBpa analogs increased crosslinking yields for weak transient interactions. Taken together, we recommend use of the 4-CF_3 analog in cases where increased crosslinking yield is needed as it is incorporated at similar levels to pBpa and produced a 23-fold increase in crosslinking yield.

Through this study, we have expanded our toolbox of chemical probes for capturing challenging PPIs in their native environment. We anticipate that these halogenated pBpa analogs will have additional downstream applications post-crosslinking and isolation. For instance, bromine and chlorine atoms have enabled quantitative proteomic analysis without the need for expensive isotopic labeling systems, such as stable isotope labeling using amino acids in cell culture (SILAC) systems.[58-59] Upon MS analysis, the protein targets can be quantified between samples using the specific chlorine or bromine isotopes to accurately identify interaction partners with minimal bias between experimental replicates. The unique isotopic signatures of these halogens could enable the identification of PPIs such as low abundance activator-coactivator interactions that may be drowned out by high abundance proteins and have eluded research efforts for years.[60] Utilizing the halogenated pBpa analogs developed will more readily facilitate the successful implementation of *in vivo* covalent capture for studying PPIs involved in a variety of biological processes.

MATERIALS AND METHODS

UAA incorporation and expression

LS41 yeast was transformed with pLexA+Gal4 849 TAG-1X Flag or pLexA+Gal4WT-1X Flag and pSNRtRNA-pBpaRS plasmids. Individual colonies were grown in 5 mL SC media containing 2% raffinose, but lacking histidine, tryptophan, and uracil for selection. The cultures were incubated at 30°C with 250 rpm agitation. Following incubation, these cultures were used to inoculate 5 mL cultures of SC media containing 2% raffinose and 2% galactose, with or without 1 mM pBpa/1 mM pBpa EWG analog (dissolved in 50 μL 1 M NaOH), and 50 μL 1 M HCl. The cultures were incubated at 30°C with agitation to an OD_{660} of 1.0. Three ODs were isolated, washed with sterile water, and stored at -20°C. The samples were lysed in 10 μL 4X NuPAGE LDS Sample loading buffer (Invitrogen), 10 μL 1X lysis buffer (50 mM Tris-Acetate pH 7.9, 100 mM potassium acetate, 20% glycerol, 0.2% Tween20, 2 mM β-mercaptoethanol, and 2 mM magnesium acetate), and 10 μL 1 M DTT by boiling at 95°C for 10 min. The samples were run on a 3-8% Tris-acetate SDS-PAGE gel and analyzed by Western blot with the anti-Flag (M2) antibody (Sigma Aldrich). Expression levels were quantified using ImageJ and relative levels of LexA-Gal4 protein for each experiment were expressed as follows ((experimental/WT LexA-Gal4)*100).

In vivo crosslinking analysis

A colony of LexA+Gal4 849 TAG-5X Flag:Gal80-6X Myc was grown in 5 mL SC media containing 2% glucose, but lacking histidine, tryptophan, leucine and uracil for selection. The cultures were incubated at 30°C with 250 rpm agitation. Following incubation, these cultures were used to inoculate 100 mL cultures of SC media containing 2% glucose, with 1 mM pBpa or 1 mM EWG pBpa analog (dissolved in 1 mL 1 M NaOH), and 100 mL 1 M HCl. The cultures were incubated at 30°C with agitation to an OD_{660} of 1.0. For each culture, the cells were isolated by centrifugation and washed with the SC media lacking histidine, tryptophan, and uracil. The cell pellets were resuspended in 2 mL SC media containing 2% glucose and then transferred to small culture dishes and subjected to UV light at 365nm (Eurosolar 15W UV lamp) with cooling for 30 minutes. The cells were isolated by centrifugation and stored at -20°C until lysis. The control samples were washed with 1 mL SC media containing 2% glucose, isolated by centrifugation, and stored at -20°C until lysis.

For lysis, cells were resuspended in 600 μL lysis buffer (50 mM HEPES – KOH pH 7.5, 140 mM NaCl, 1 mM EDTA, 1% Triton X-100, 0.1% Na-Deoxycholate and 2X Complete Mini, EDTA Free Protease Inhibitor (Roche)) and lysed using glass beads by vortexing at 4°C. Subsequently, the lysate was pelleted and the supernatant incubated with anti-LexA antibody (sc-1725, Santa Cruz Biotechnologies) for 2 hours at 4°C for immunoprecipitation. The proteins bound to the antibody were isolated by incubation for 1 hour with 40 μL pre-washed Dynabeads® protein G magnetic beads (ThermoFisher) at 4°C. After immunoprecipitation, the

beads were washed six times with 1 mL Wash Buffer (10 mM Tris-HCl pH 8.0, 250 mM LiCl, 0.5% NP-40, 0.1% Na-Deoxycholate, and 1 mM EDTA) and stored at -20°C until elution.

The samples were eluted from the beads by heating at 95°C for 10 minutes in 10 µL NuPAGE 4X LDS Sample Loading Buffer (Invitrogen), 10 µL water, and 10 µL 1M DTT. The samples were run on a 4-15% Mini-PROTEAN® TGX™ pre-cast SDS-PAGE gel (Bio-Rad). The gel was transferred to immobilin PDVF membrane (Millapore) and blocked for 1 hour at room temperature using SuperBlock™ (PBS) Blocking Buffer (ThermoFisher). The membrane was incubated with both mouse anti-Flag (M2) (Sigma Aldrich, F1804) and rabbit anti-cMyc (Sigma Aldrich, C3956) primary antibodies overnight at 4^{o}C. The membrane was washed three times for 10 minutes each with PBS-T (10 mM $Na_2HPO_4 \bullet 7H_2O$, 1.7 mM KH_2PO_4, 140 mM NaCl, 3 mM KCl, 0.05% Tween-20, pH 7.4), followed by incubation with anti-mouse 680nm (LI-COR, 926-68072) and anti-rabbit 800nm (LI-COR, 926-32211) secondary antibodies for 1 hour at room temperature. The membrane was washed three times for 10 minutes each with PBS-T, 5 minutes with PBS (10 mM $Na_2HPO_4 \bullet 7H_2O$, 1.7 mM KH_2PO_4, 140 mM NaCl, 3 mM KCl, pH 7.4), and visualized using an Azure c600 western blot imager (Azure Biosystems).

***In vitro* crosslinking analysis**

Med25 AcID 6x-His was diluted in binding buffer (25 mM HEPES, 40 mM KCl, 8 mM MgCl2, 100 mM NaCl, 0.01% Tween-20, pH 7.4) to 22 µM, and biotin labeled VP16 peptides

were diluted to 25% of their Kd values in binding buffer. Equivalent volumes of Med25 AcID and peptide were incubated at room temperature for 30 minutes in a clear, flat bottom, polystyrene, 96-well plates (Fisherbrand). The solutions were irradiated with UV light at 365nm (Eurosolar 15W UV lamp) with cooling for 10 minutes. 15 μL of each sample was mixed with 5 μL NuPAGE 4X LDS Sample Loading Buffer (Invitrogen) and boiled for 5 minutes. The samples were run on a 4-20% Mini-PROTEAN® TGX™ pre-cast SDS-PAGE gel (Bio-Rad). The gel was transferred to PDVF membrane (Bio-Rad) and blocked for 1 hour at room temperature with SuperBlock™ (PBS) Blocking Buffer (ThermoFisher). The membrane was incubated with 1:100 diluted anti-HIS HRP conjugated antibody (Santa Cruz sc-8036 HRP) for 1 h at room temperature. The membrane was washed three times for 10 minutes each with PBS-T (10 mM $Na_2HPO_4 \bullet 7H_2O$, 1.7 mM KH_2PO_4, 140 mM NaCl, 3 mM KCl, 0.05% Tween-20, pH 7.4), and visualized with SuperSignal West Femto ECL substrate (ThermoFisher) using an Azure c600 western blot imager (Azure Biosystems). The membrane was washed three times with PBS-T then stripped by incubating in Restore western blot stripping buffer (ThermoFisher) for 45 minutes at 37^{o}C. The membrane was washed three times with PBS-T then incubated with 1:2000 diluted HRP-conjugated streptavidin (Abcam 7403) for 1 hour at room temperature. The membrane was washed three times for 10 minutes each with PBS-T and visualized with SuperSignal West Femto ECL substrate (ThermoFisher) using an Azure c600 western blot imager (Azure Biosystems). Crosslinking yields were quantified using ImageJ. The relative amount of Med25-VP16 crosslinked product for each sample was normalized based on the

protein levels of Med25 in the HIS-HRP blot. The fold changes were expressed as follows (Med25-VP16 F442UAA crosslinked product / Med25-VP16 F442Bpa crosslinked product)

Supplementary Material

Additional supplemental figures, detailed experimental methods, and compound characterization can be found in the Supporting Information.

Acknowledgments

We are grateful for the NSF CHE 1412759 for support of this work. M. Breen is a Howard Hughes Medical Institute Fellow of the Life Sciences Research Foundation. We thank Dr. James Clayton and Dr. Rachel Pricer for constructive feedback and Julie Garlick and Kevon Stanford for experimental assistance.

References

1. Mapp AK, Pricer R, Sturlis S (2015) Targeting transcription is no longer a quixotic quest. Nat Chem Biol 11:891-894.
2. Cesa LC, Mapp AK, Gestwicki JE (2015) Direct and propagated effects of small molecules on protein–protein interaction networks. Front Bioengin Biotech 3:119.
3. Arkin M (2005) Protein–protein interactions and cancer: small molecules going in for the kill. Curr Opin Chem Biol 9:317-324.
4. Lage K (2014) Protein-protein interactions and genetic diseases: the interactome. Biochim Biophys Acta 1842:1971-1980.
5. Berggård T, Linse S, James P (2007) Methods for the detection and analysis of protein–protein interactions. Proteomics 7:2833-2842.

6. Surade S, Blundell TL (2012) Structural biology and drug discovery of difficult targets: the limits of ligandability. Chem Biol 19:42-50.
7. Perkins JR, Diboun I, Dessailly BH, Lees JG, Orengo C (2010) Transient protein-protein interactions: structural, functional, and network properties. Structure 18:1233-1243.
8. Hayes S, Malacrida B, Kiely M, Kiely PA (2016) Studying protein–protein interactions: progress, pitfalls and solutions. Biochem Soc Trans 44:994.
9. Legrain P, Rain JC (2014) Twenty years of protein interaction studies for biological function deciphering. J Proteomics 107: 93-97.
10. Liu CC, Schultz PG (2010) Adding new chemistries to the genetic code. Ann Rev Biochem 79:413-444.
11. Liu Z, Myers LC (2012) Med5(Nut1) and Med17(Srb4) are direct targets of mediator histone H4 tail interactions. PLoS ONE 7:e38416.
12. Yu D, Wowor AJ, Cole JL, Kendall DA (2013) Defining the Escherichia coli SecA dimer interface residues through in vivo site-specific photo-cross-linking. J Bacteriol 195:2817-2825.
13. Berg M, Michalowski A, Palzer S, Rupp S, Sohn K (2014) An in vivo photo-cross-linking approach reveals a homodimerization domain of Aha1 in S. cerevisiae. PLoS ONE 9:e89436.
14. Tanaka Y, Bond MR, Kohler JJ (2008) Photocrosslinkers illuminate interactions in living cells. Mol BioSyst 4:473.
15. Chin JW (2017) Expanding and reprogramming the genetic code. Nature 550:53-60.
16. Young DD, Schultz PG (2018) Playing with the molecules of life. ACS Chem Biol 13:854-870.
17. Italia JS, Zheng Y, Kelemen RE, Erickson SB, Addy PS, Chatterjee A (2017) Expanding the genetic code of mammalian cells. Biochem Soc Trans 45:555-562.
18. Italia JS, Addy PS, Wrobel CJJ, Crawford LA, Lajoie MJ, Zheng Y, Chatterjee A (2017) An orthogonalized platform for genetic code expansion in both bacteria and eukaryotes. Nat Chem Biol 13:446-450.
19. Coin I (2018) Application of non-canonical crosslinking amino acids to study protein–protein interactions in live cells. Curr Opin Chem Biol 46:156-163.
20. Nguyen TA, Cigler M, Lang K (2018) Expanding the genetic code to study protein–protein interactions. Angew Chem Intl Ed 57:14350-14361.
21. Yang Y, Song H, Chen PR (2016) Genetically encoded photocrosslinkers for identifying and mapping protein-protein interactions in living cells. IUBMB Life 68:879-886.
22. Neumann-Staubitz P, Neumann H (2016) The use of unnatural amino acids to study and engineer protein function. Curr Opin Struct Biol 38:119-128.
23. Miyazaki R, Myougo N, Mori H, Akiyama Y (2018) A photo-cross-linking approach to monitor folding and assembly of newly synthesized proteins in a living cell. J Biol Chem 293:677-686.

24. Yeh FL, Tung L, Chang TH (2016) Detection of protein–protein interaction within an RNA–protein complex via unnatural-amino-acid-mediated photochemical crosslinking. In RNA-Protein Complexes and Interactions: Methods and Protocols, Springer, pp 175-189.
25. Mohibullah N, Hahn S (2008) Site-specific cross-linking of TBP in vivo and in vitro reveals a direct functional interaction with the SAGA subunit Spt3. Genes Develop 22:2994-3006.
26. Wu CC, Lin YC, Chen HT (2011) The TFIIF-like Rpc37/53 dimer lies at the center of a protein network to connect TFIIIC, Bdp1, and the RNA polymerase III active center. Mol Cell Biol31:2715-2728.
27. Chen HT, Warfield L, Hahn S (2007) The positions of TFIIF and TFIIE in the RNA polymerase II transcription preinitiation complex. Nat Struct Mol Biol14:696-703.
28. Hino N, Okazaki Y, Kobayashi T, Hayashi A, Sakamoto K, Yokoyama S (2005) Protein photo-cross-linking in mammalian cells by site-specific incorporation of a photoreactive amino acid. Nat Meth 2:201-206.
29. Majmudar CY, Wang B, Lum JK, Håkansson K, Mapp AK (2009) A high-resolution interaction map of three transcriptional activation domains with a key coactivator from photo-cross-linking and multiplexed mass spectrometry. Angew Chem Intl Ed 48:7021-7024.
30. Majmudar CY, Lee LW, Lancia JK, Nwokoye A, Wang Q, Wangs AM, Wang L, Mapp AK (2009) Impact of nonnatural amino acid mutagensis on the in vivo function and binding modes of a transcriptional activator. J Am Chem Soc 131:14240-14242.
31. Krishnamurthy M, Dugan A, Nwokoye A, Fung YH, Lancia JK, Majmudar CY, Mapp AK (2011) Caught in the act: covalent cross-linking captures activator–coactivator interactions in vivo. ACS Chem Biol 6:1321-1326.
32. Dugan A, Majmudar CY, Pricer R, Niessen S, Lancia JK, Fung HY, Cravatt BF, Mapp AK (2016) Discovery of enzymatic targets of transcriptional activators via in vivo covalent chemical capture. J Am Chem Soc 138:12629-12635.
33. Jaya N, Garcia V, Vierling E (2009) Substrate binding site flexibility of the small heat shock protein molecular chaperones. Proc Natl Acad Sci USA 106:15604-15609.
34. Raju M, Santhoshkumar P, Sharma KK (2012) αA-crystallin–derived mini-chaperone modulates stability and function of cataract causing αAG98R-crystallin. PLoS ONE 7:e44077.
35. Dorman G, Prestwich GD (1994) Benzophenone photophores in biochemistry. Biochemistry 33:5661-5673.
36. Dormán G, Nakamura H, Pulsipher A, Prestwich GD (2016) The life of pi star: exploring the exciting and forbidden worlds of the benzophenone photophore. Chem Rev 116:15284-15398.
37. Boscá F, Miranda MA (1998) Photosensitizing drugs containing the benzophenone chromophore. J Photochem Photobiol B Biol 43:1-26.

38. Demeter A, Horváth K, Böőr K, Molnár L, Soós T, Lendvay G (2013) Substituent effect on the photoreduction kinetics of benzophenone. J Phys Chem A 117:10196-10210.
39. Klán P, Wirz J (2009) Introduction in photochemistry of organic compounds. John Wiley & Sons, Ltd, pp 1-23.
40. Wang Q, Wang L (2008) New methods enabling efficient incorporation of unnatural amino acids in yeast. J Am Chem Soc 130:6066-6067.
41. Liu W, Alfonta L, Mack AV, Schultz PG (2007) Structural basis for the recognition of para-benzoyl-L-phenylalanine by evolved aminoacyl-tRNA synthetases. Angew Chem Intl Ed 46:6073-6075.
42. Joiner CM, Breen ME, Clayton J, Mapp AK (2017) A bifunctional amino acid enables both covalent chemical capture and isolation of in vivo protein–protein interactions. ChemBioChem 18:181-184.
43. Ahlburg A, Lindhardt AT, Taaning RH, Modvig AE, Skrydstrup T (2013) An air-tolerant approach to the carbonylative suzuki–miyaura coupling: applications in isotope labeling. J Organ Chem 78:10310-10318.
44. Stokes AL, Miyake-Stoner SJ, Peeler JC, Nguyen DP, Hammer RP, Mehl RA (2009) Enhancing the utility of unnatural amino acid synthetases by manipulating broad substrate specificity. Mol BioSyst 5:1032.
45. Miyake-Stoner SJ, Refakis CA, Hammill JT, Lusic H, Hazen JL, Deiters A, Mehl RA (2010) Generating permissive site-specific unnatural aminoacyl-tRNA synthetases. Biochemistry 49:1667-1677.
46. Young DD, Jockush S, Turro NJ, Schultz PG (2011) Synthetase polyspecificity as a tool to modulate protein function. Bioorgan Med Chem Lett 21:7502-7504.
47. Tuley A, Wang YS, Fang X, Kurra Y, Rezenom YH, Liu WR (2014) The genetic incorporation of thirteen novel non-canonical amino acids. Chem Commun 50:2673-2675.
48. Wang YS, Fang X, Wallace AL, Wu B, Liu WR (2012) A rationally designed pyrrolysyl-tRNA synthetase mutant with a broad substrate spectrum. J Am Chem Soc 134:2950-2953.
49. Thoden JB, Ryan LA, Reece RJ, Holden HM (2008) The interaction between an acidic transcriptional activator and its inhibitor: the molecular basis of Gal4p recognition by Gal80p. J Biol Chem 283:30266-30272.
50. Ansari AZ, Reece RJ, Ptashne M (1998) A transcriptional activating region with two contrasting modes of protein interaction. Proc Natl Acad Sci USA 95:13543-13548.
51. Hashimoto H, Kikuchi Y, Nogi Y, Fukasawa T (1983) Regulation of expression of the galactose gene cluster in Saccharomyces: isolation and characterization of the regulatory gene Gal4. Mol General Genet 191:31-38.
52. Milbradt AG, Kulkarni M, Yi T, Takeuchi K, Sun ZYJ, Luna RE, Selenko P, Näär AM, Wagner G (2011) Structure of the VP16 transactivator target in the Mediator. Nat Struct Mol Biol 18:410-415.

53. Vojnic E, Mourão A, Seizl M, Simon M, Wenzeck L, Larivière L, Baumli S, Baumgart K, Meisterernst M, Sattler M, Cramer P (2011) Structure and VP16 binding of the Mediator Med25 activator interaction domain. Nat Struct Mol Biol 18:404-409.
54. Ansari AZ, Mapp A, Nguyen DH, Dervan PB, Ptashne M (2001) Towards a minimal motif for artificial transcriptional activators. Chem Biol 8:583-592.
55. Seipel K, Georgiev O, Schaffner WA (1994) minimal transcription activation domain consisting of a specific array of aspartic acid and leucine residues. Biol Chem 375:663-470.
56. Cress W, Triezenberg S (1991) Critical structural elements of the VP16 transcriptional activation domain. Science 251:87-90.
57. Mittler G, Stühler T, Santolin L, Uhlmann T, Kremmer E, Lottspeich F, Berti L, Meisterernst M (2003) A novel docking site on Mediator is critical for activation by VP16 in mammalian cells. EMBO J 22:6494-6504.
58. Chen X, Wei S, Ji Y, Guo X, Yang F (2015) Quantitative proteomics using SILAC: principles, applications, and developments. Proteomics 15:3175-3192.
59. Kaake RM, Wang X, Huang L (2010) Profiling of protein interaction networks of protein complexes using affinity purification and quantitative mass spectrometry. Mol Cell Proteomics 9:1650-1665.
60. Palaniappan KK, Pitcher AA, Smart BP, Spiciarich DR, Iavarone AT, Bertozzi CR (2011) Isotopic signature transfer and mass pattern prediction (IsoStamp): an enabling technique for chemically-directed proteomics. ACS Chem Biol 6:829-836.

Figure Legends

Figure 1. (A) Covalent chemical capture mechanism of pBpa. Upon irradiation with 365 nm UV light, pBpa reversibly forms a diradical species. If an activated C-H bond is available, hydrogen atom abstraction followed by radical recombination will yield the crosslinked adduct. (B) A series of pBpa analogs with halogen substituents either meta or para to the carbonyl group were prepared. (C) Synthesis of halogenated pBpa analogs. Full experimental details and compound characterization can be found in the Supporting Information.

Figure 2. *In vivo* incorporation of Halo-Bpa analogs. (A) Position 849 was mutated to the amber stop codon (TAG) for UAA incorporation within the LexA+Gal4 chimeric transcriptional activator. A C-terminal Flag tag was appended for visualization. (B-E) Incorporation of the Halo-Bpa analogs into LexA+Gal4 849TAG in the presence or absence of 1 mM UAA. Loading control is an endogenous yeast protein that consistently comes out with Flag visualization. (F) Relative expression levels of the Halo-Bpa analogs compared to pBpa. Expression levels of LexA+Gal4 849UAA mutants relative to LexA+Gal4 WT were quantified by using ImageJ.

Figure 3. LexA+Gal4 849UAA *in vivo* crosslinking. (A) Experimental scheme of *in vivo* covalent chemical capture of Gal4 binding partners. (B) 3-F and 4-F Bpa capture Gal4's endogenous binding partners (red) and the Gal4-Gal80 interaction (yellow) when irradiated with UV light.

Figure 4. VP16 (441-448) F442UAA *in vitro* crosslinking. Each Halo-Bpa analog had increased crosslinking yield for the Med25-VP16 adduct compared to pBpa upon UV irradiation. (A) Western blot visualization of 6XHis+Med25:Biotin+VP16 F442UAA *in vitro* crosslinking. Crosslinked adducts visualized with Streptavidin-HRP and Med25 loading visualized with anti-HIS-HRP antibody. (B) Relative fold change in Halo-Bpa crosslinking yields compared to pBpa from 6XHis+Med25:Biotin+VP16 F442UAA western blot. The yields are an average of two replicates. Crosslinking yields were quantified using ImageJ. The relative amount of Med25-VP16 crosslinked adducts for each sample was normalized based on the protein levels of Med25 in the HIS-HRP blot. The fold changes were expressed as follows (Med25-VP16 F442UAA crosslinked product / Med25-VP16 F442Bpa crosslinked product).

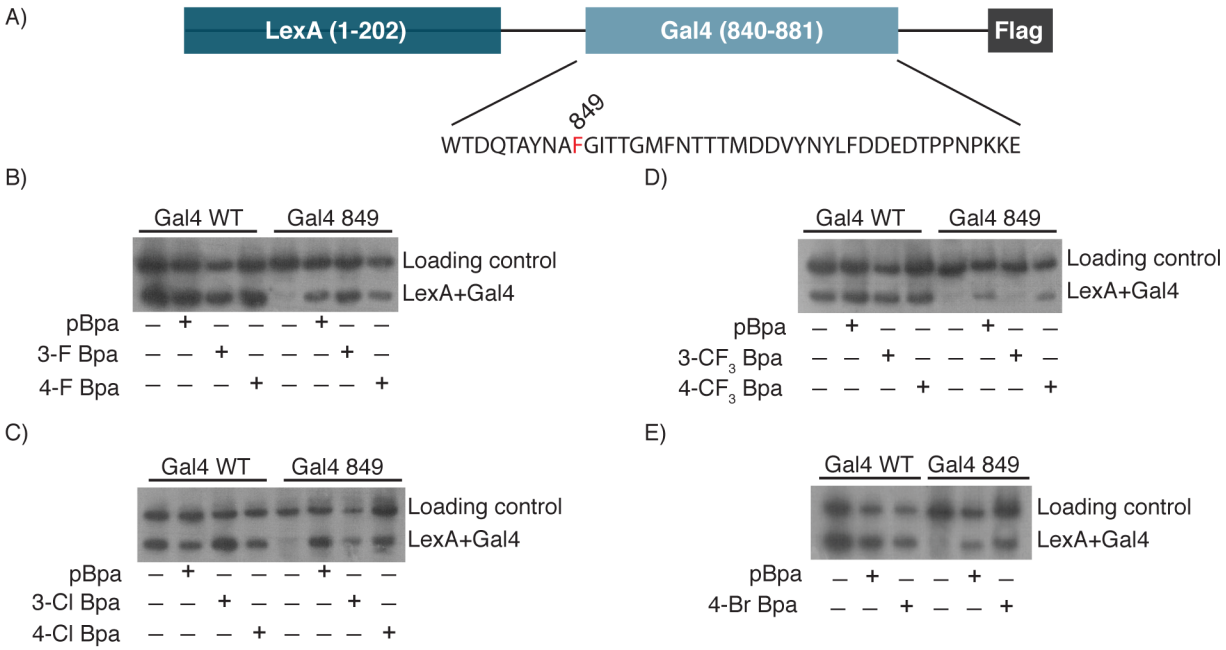

F)

	pBpa	3-F Bpa	4-F Bpa	3-Cl Bpa	4-Cl Bpa	3-CF_3 Bpa	4-CF_3 Bpa	4-Br Bpa
Relative Expression	1.00	1.80	1.50	0.28	0.64	0.02	1.30	0.80

PRO_3621_HaloBpa_Figure2_Joineretal.tif

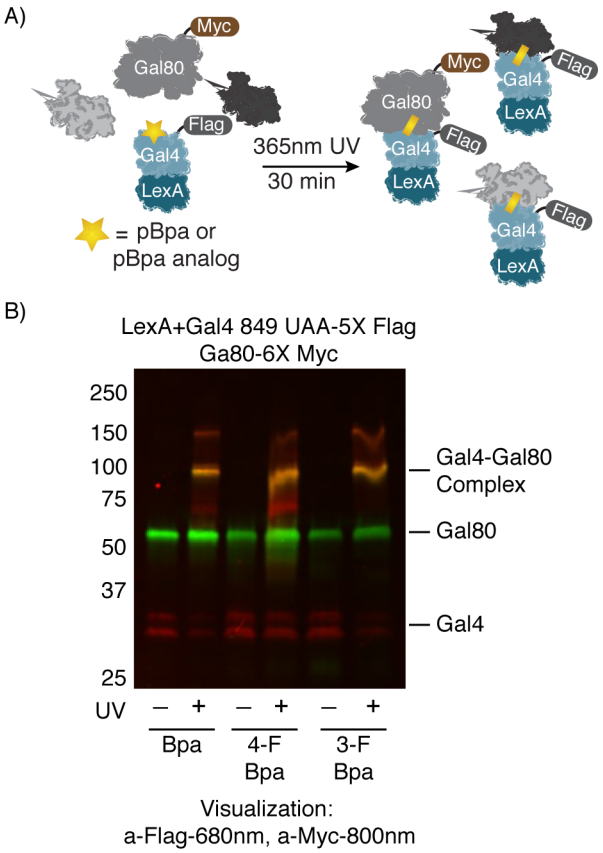

PRO_3621_HaloBpa_Figure3_Joineretal.tif

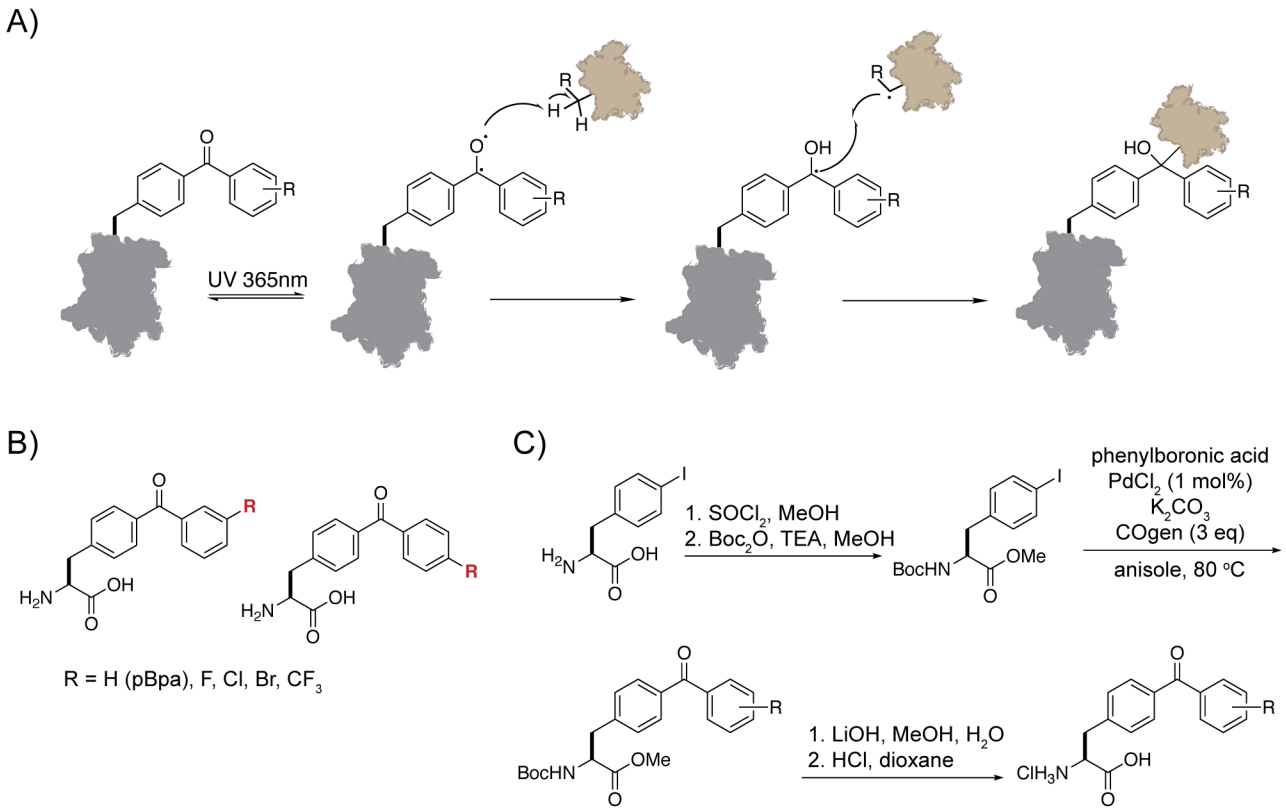

PRO_3621_HaloBpa_Figure 1_Joineretal.tif

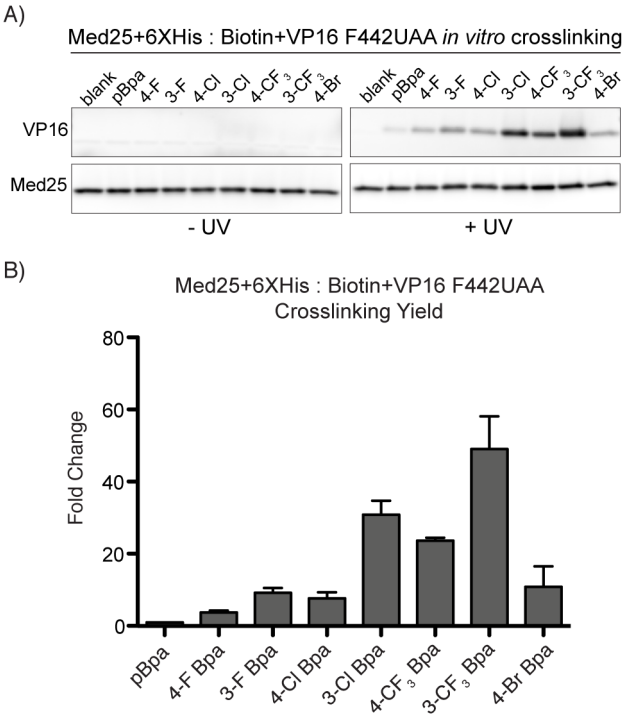

PRO_3621_HaloBpa_Figure 4_Joineretal.tif